Imaging Through Turbulence: A Light-Field Approach

Jeremy P. Bos
Department of Electrical and Computer Engineering
Michigan Technological University

Abstract

In contrast to traditional imaging techniques, light-field imaging systems records variations in intensity from points in a scene as a function of angle. In the context of computational photography, light-field processing allows for image reconstruction from multiple viewpoints and different depths of focus. It is increasingly recognized that certain wave front sensing techniques are essentially light-field capture techniques. In this work, we compare light-field processing techniques to traditional imaging in the context of imaging through turbulence. Our goal is to understand the effect of turbulence on captured light-field and if light-field processing techniques may offer a way to overcome turbulence effects that are resistant to traditional methods. Specifically, we aim to understand how light-field techniques may provide angular diversity to overcome the effects of extreme anisoplanatism.

1. INTRODUCTION

Extreme anisoplanatism refers to conditions where the turbulence-induced imaging distortions are shift-variant over the imaging Instantaneous Field of View (IFOV). Extreme anisoplanatism is different from classical imaging through turbulence scenarios where distortions are assumed to be shift-invariant. This assumption holds in the classic imaging through turbulence scenarios because the imaging system is pointed upward- usually only no more than thirty degrees away from nadir. Here the effects of a turbulence volume can be modeled as a single phase disturbance applied to the aperture. As the look angle increases toward horizontal the integrated turbulence strength increases and the isoplanatic angle, the angle over which the linear, shift-invariant assumption holds, decreases. Consequently, a single phase disturbance no longer accurately models the effects of the turbulence volume and turbulence effects vary as a function of viewing angle. In general, the effect of increasing turbulence strength is to blur or distort in the image. However, when anisoplanatism is extreme, it is possible to have a small isoplanatic patch without significant turbulence-induced image blur; especially for modest aperture sizes. These conditions are common when imaging over long horizontal or slant paths. In imaging space objects from the ground, extreme anisoplanatism is encountered when observing systems are pointed near-to the horizon. Here the turbulence volume may extend over one hundred kilometers or more and both the integrated turbulence strength, in terms of the Fried parameter, and isoplanatic angle will be small.

Most turbulence mitigation methods are ineffective in scenarios characterized by extreme anisoplanatism. Adaptive Optics (AO) systems can only correct for turbulence effects when the field of view is on the order of the isoplanatic patch size; far too small to be useful. Multi-conjugate systems may widen the field of view but are complex, costly, and unlikely to be of practical use. Post or online-processing via Multi-Frame Blind Deconvolution (MFBD) and Speckle Imaging (SI) techniques are another strategy for overcoming turbulence effects. Both have shown favorable results when imaging in extreme anisoplanatism [1, 2]. These techniques, particularly MFBD, can also benefit from including WFS information. Though, similar to AO, the primary benefit appears to be correction on-axis [3] within the isoplanatic patch. It stands to reason that a volumetric WFS married to MFBD may provide correction over the entire IFOV such as suggested by Jefferies, et al [4]. The development of volumetric WFS systems is an active area of research and a full review is beyond the scope of this work.

In this work, I am interested in taking the first steps in understanding how light-field techniques may be applied to the imaging through turbulence problem and extreme anisoplanatism specifically. The concept of the light field is not new. In fact, the origins of the idea go back to 1908 and Lippman's Integral Photography [5]. The modern idea of the Light-Field (LF) originates with Adelson and Wang [6] in the area of computer graphics. The topic has matured in recent years due in part to work by Ng [7] and his development of a hand-held plenoptic camera. The basic idea of the modern LF approach is the application of a number of simplifying assumptions to describe the angular-spatial distribution of light in a volume. Modern LF representations, such as the two-plane parameterization,

include two angular and two spatial dimensions. Thus, the LF extends an image from two to four dimensions. As in the case with traditional imaging a fifth dimension can be added to include variation over wavelength. LF capture then refers to the recording of the LF and can be accomplished using a camera array or the aforementioned plenoptic camera and associated variations.

LF capture allows for a number of novel applications. For example, post-processing the LF allows a user to change the viewpoint, depth of field, and focus dynamically. These post-processing tasks are not possible via traditional imaging but are straight-forward via LF processing. Recently, it was also shown that by using the full LF it is possible to blindly deconvolve both in and out of plane motion-induced blur [8] to a degree not possible using a flat (2-D) image. Other applications of LF processing include occlusion removal, imaging in low-contrast environments, and generating disparity maps for machine vision applications.

It stands to reason, then, if having access to the full LF (or an adequately sampled version of the LF) allows us to dynamically refocus images when configured as a camera it might also us to tomographically reconstruct the atmospheric phase distortions volumetrically in imaging through turbulence scenarios. Indeed, the plenoptic camera, as described by Ng [7], positions a Micro-Lens Array (MLA) one focal length from the main lens. In terms of construction, the plenoptic camera is a modification to the popular Shack-Hartmann WFS. By way of operation, the plenoptic camera is actually closer in design to the Pyramid WFS (PWFS) [9]. Roughly stated, the PWFS is equivalent to a plenoptic camera with four element MLA. Other variations on the plenoptic camera have been suggested for use as WFS in solar astronomy [10, 11]. In all of these cases, the plenoptic camera is used for wavefront phase reconstruction with the intent of providing commands to a Deformable Mirror (DM) in an AO system; the work by Wu and Dainty being a notable exception [12]. The question remains, can we work with a captured LF directly for the purpose of image reconstruction and volumetric wavefront sensing?

As a first step in providing an answer to this question I explore the answer to a different question. Specifically, can we extend our knowledge of the effects of atmospheric turbulence on imaging to describe the effect of turbulence on the LF? The fundamental description of the effect of turbulence in traditional imaging scenarios begins with mean squared difference in the phase as a function of position within the aperture: the wave structure function. A similar description of the effect of turbulence on the LF would add angle as a variable. In [13] Fried describes what he calls the Hyper-Wave Structure Function (HWSF), this quantity describes the mean-squared difference in phase a function of both position and angle. Fried uses this quantity to evaluate the anisoplanatic atmospheric Power Spectral Density (PSD) and Cross-Spectrum transfer functions for two point sources assuming vertical viewing. In this work, I evaluate the HWSF for several scenarios with the aim of understanding the effect of turbulence on the LF and, in particular when anisoplanatism is extreme.

The remainder of this paper is organized as follows. In the next section, I compare LF and traditional imaging techniques as they apply to imaging space object from the ground. From this standpoint, I argue that the representation of the HWSF is effectively described the effect of turbulence on the LF. From there, I extend Fried's work from [13] and [14] and provide an intermediate result that can be evaluated numerically. Next, I evaluate this expression for two scenarios with the similar integrated turbulence strengths but with varied levels of anisoplanatism. I find that when the HWSF is evaluated as a function of angle when separation is held constant the expected mean squared phase difference decreases following a power-law of approximately 0.8. When angle is held constant and mean-squared difference in phase increases with the square of separation. No difference is observed between isoplanatic and anisoplanatic scenarios over the range of values examined.

2. BACKGROUND

The modern description of the LF is a five dimensional quantity with two angular dimensions and two spatial dimensions, a fifth dimension allows the sample point to move through three dimensional space. A popular simplification of this representation uses two planes separated by a fixed distance allowing a description LF at some fixed point in the space by the intersection of rays from an angular (u,v) plane to a spatial (x,y) plane over some arbitrary fixed distance and resulting in a four dimensional LF representation, $L_F(u,v,x,y)$. The two-planes, described graphically in Fig. 1, use the geometric optics approximation and also, generally, assumes that rays arriving at the (u,v) plane are unobstructed along their length. Here, I am interested in near-field effects on the LF by volumetric turbulence in the case where the object is very far from the imaging system.

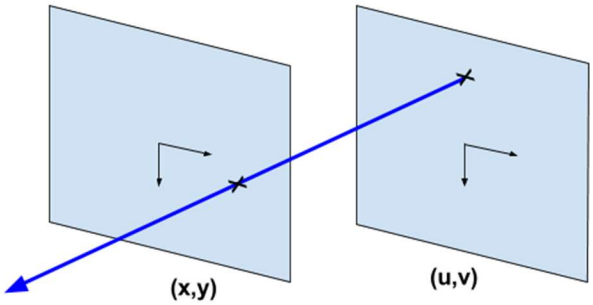

Fig. 1. Visualization of the two-plane parametrization description of the LF. In this description the LF at any point (here the center of the optical axis of the imaging system main lens) the LF can be described by the rays that intersect two planes with a constant separation. The intensity of the ray does not change along its length.

In a traditional camera, an image the main lens created an image, $I(x,y)$, by integrating over the LF over the angular dimensions.

$$I(x,y) = \int\int L_F(u,v,x,y)dudv \tag{1}$$

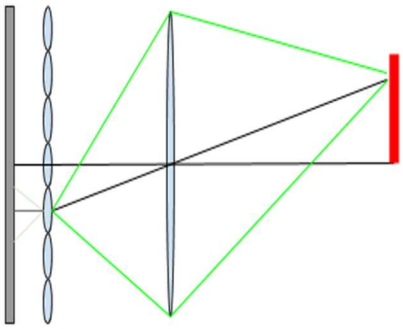

Fig. 2. Rough ray diagram sketch showing demonstrating how a plenoptic camera captures the LF. In a normal camera all of the rays emanating from a point on the red bar indicated by the black line span the angle space bounded by the green lines. In a traditional imaging, these rays are focused at an imaging sensor located at the focal plane. In a plenoptic camera a MLA placed at the focal plane allows for analysis of the ray space as a function of angle.

In Fig.2 you can visualize this process by replacing the MLA with an imaging sensor. In contrast, what is captured by a LF camera, behind the MLA in Fig. 2, allows both spatial and angular sampling of the LF.

In the case of imaging a space object from the ground, in the absence of turbulence, all of the rays would arrive at the imaging system in parallel as a plane wave. In our plenoptic imaging system these rays would result in a single point (a diffraction limited spot), sampling the spatial variation in intensity over the IFOV. Adding turbulence to this scenario would add an angular component spreading intensity to the off-axis pixels behind the MLA in Fig.2. In theory, with an extended object, it should be possible to analyze this angular component and reconstruct the phase effect of the volume turbulence in front of the imaging system. Missing from this discussion, currently, is a model for the effect of volume turbulence on the LF that matches our, very mature, models of the effects of turbulence in traditional imaging.

Our understanding of the effect of atmospheric turbulence on imaging is enabled by a statistical description of the mean-squared difference in temperature between two points in a turbulence volume. This is the famous ⅔ power law description of the turbulent energy cascade and has a parallel in the variations of index of refraction as shown by

Tatarskii [15]. Fried leveraged this work to develop a theory of the limits on the long and short exposure imaging [16] and later limits on the performance of the corrected IFOV of AO systems in terms of the isoplanatic angle [17]. A few years later, in response to results some surprising result from the solar speckle interferometry community, Fried analyzed the performance of SI techniques in the presence of anisoplanatism [13]. Albeit, with a focus on large values of D/r_0 in nadir pointing conditions. In this work, Fried coined the term Hyper-Wave Structure Function (HWSF) to describe the mean-squared difference in the phase as a function of separation and angle. In [13] this quantity is given as

$$HWSF(\vec{\vartheta},\vec{\rho}) = 8.16\left(\frac{k^2}{2\pi}\right)\int_0^L C_n^2(z)\int_0^\infty \left[\begin{array}{l} 1-\exp\left\{jk\vec{\kappa}\cdot\vec{\rho}\right\} \\ \times\vec{\kappa}^{-11/3}\left(\exp\left\{j\vec{\kappa}\cdot\vec{\vartheta}\right\}+\exp\left\{-j\vec{\kappa}\cdot\vec{\vartheta}\right\}\right)\end{array}\right] d\vec{\kappa}\,dz \tag{2}$$

Applying the assumptions of isotropy and with some simplification the Eq.(2) can be simplified as

$$HWSF(\vartheta,\rho) = 8.16k^2\int_0^L C_n(z)\int_0^\infty \kappa^{-8/3}\left[2J_0(\kappa\vartheta z)-J_0(\rho+\vartheta z)-J_0(\rho-\vartheta z)\right]d\kappa\,dz \tag{3}$$

Unfortunately, the integral $\int_0^\infty \kappa J_0(\kappa x)d\kappa$ is non-integrable. A common way around this difficulty in similar integrations is to limit the bounds of integration to the inertial sub-range between the outer, L_0 and inner, l_0, scales. After making this change, we can perform the integral in Eq.(3) numerically. The results of this evaluation for two scenarios are found in the next section.

3. RESULTS

Eq. (3) was evaluated in two scenarios. One representing a typical nadir observation starting from 3000 m and extending up for 25 km using the 'Maui3' C_n^2 profile. The second a horizontal viewing scenario over 25 km using constant C_n^2. In both cases, the imaging wavelength was set to $\lambda = 1000\ \mu\text{m}$. Three conditions were considered for each scenario. Computed values for the Fried parameter, r_0, and isoplanatic angle, θ_0, in these conditions are summarized below in Tables 1 and 2 below.

Table 1. Derived turbulence parameters mountaintop scenario

Turbulence Profile	r_0 (cm)	θ_0 (μradians)
½ x Maui 3	45.0	33
Maui 3	29.7	21.8
2 x Maui 3	19.6	14.4

Table 2. Derived turbulence parameters horizontal viewing scenario

Constant Turbulence Strength $(\text{m}^{-2/3})$	r_0 (cm)	θ_0 (μradians)
10^{-17}	42.4	9.6
2×10^{-17}	28.0	6.3
5×10^{-17}	16.2	3.7

Eq. (3) was evaluated for both scenarios while keeping either angular or spatial separation constant. In Fig.3, 4, 5, and 6 spatial separation is fixed at ρ = 0.001, 0.01, 0.1, and 0.7 m. All figures are plotted on a log-log scale. Comparing, first, the isoplanatic (mountaintop) and anisoplanatic (horizontal) cases only a bulk shift between the

two conditions is observed with the anisoplanatic condition showing a larger phase difference. This phase difference is inversely proportion to the isoplanatic angle value. In Fig. 3, 4, and 5 a clear power-law behavior, measured as approximately -0.8 is observed. Though, in Fig. 6 a change the behavior changes. Over approximately the first half of the range the mean-squared phase difference is flat but then decreases again after. Though not shown here this characteristic appears to set in around $\rho \approx r_0$. A more detailed study would be required to verify this observation and its appearance near the Fried coherence diameter.

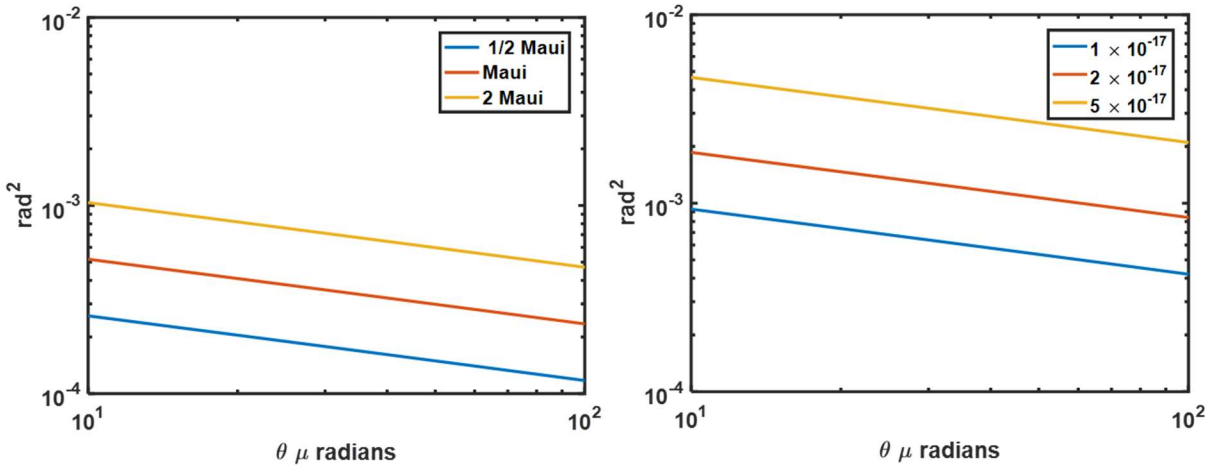

Fig. 3. HWSF evaluated for the isoplanatic (left) and anisoplanatic (right) conditions described in Table 1 and 2. In this figure angular separation is varied while the spatial separation is small, $\rho = 0.001$ m.

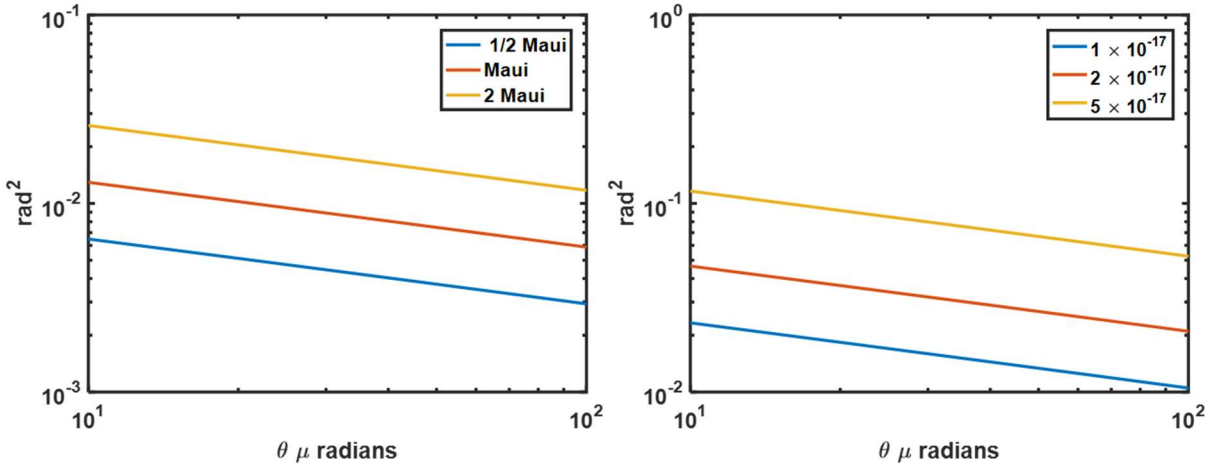

Fig. 4. HWSF evaluated for the isoplanatic (left) and anisoplanatic (right) conditions described in Table 1 and 2. In this figure angular separation is varied while the spatial separation is $\rho = 0.01$ m.

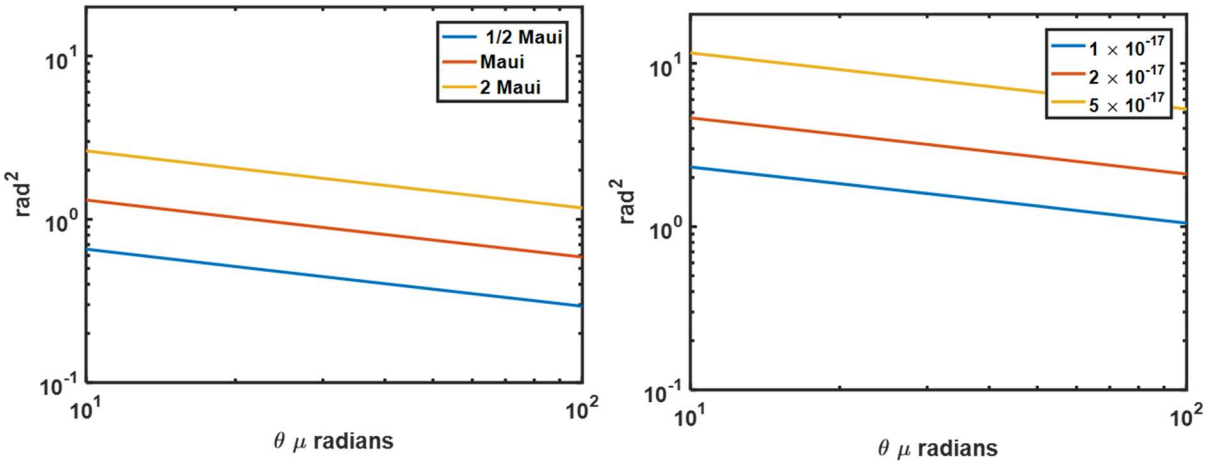

Fig. 5. HWSF evaluated for the isoplanatic (left) and anisoplanatic (right) conditions described in Table 1 and 2. In this figure angular separation is varied while the spatial separation is $\rho = 0.1$ m .

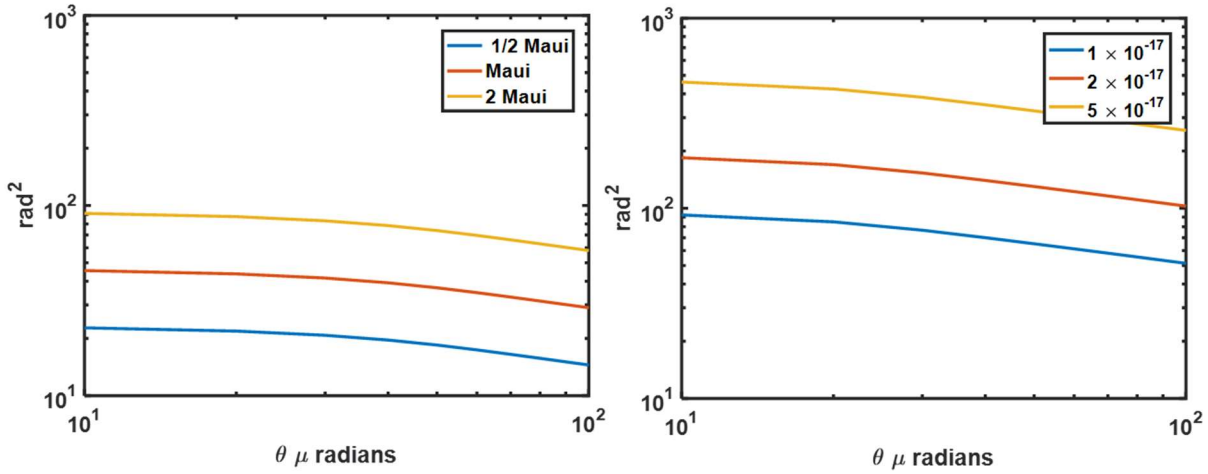

Fig. 6. HWSF evaluated for the isoplanatic (left) and anisoplanatic (right) conditions described in Table 1 and 2. In this figure angular separation is varied while the spatial separation is large, $\rho > r_0$.

In Fig.7 through 10 the separation angle is held constant and, instead, spatial separation is varied. In this case, the HWSF increases approximately to the square of the separation. Though, due to inaccuracies in the numerical integration and poor sampling, this may very well be a 5/3 power law. A shift between the isoplanatic and anisoplanatic scenarios is also observed but here attributable to difference in the values of r_0 rather than θ_0. The overall mean-squared phase decreases as angle increases, consistent the results in Fig.3 to 6.

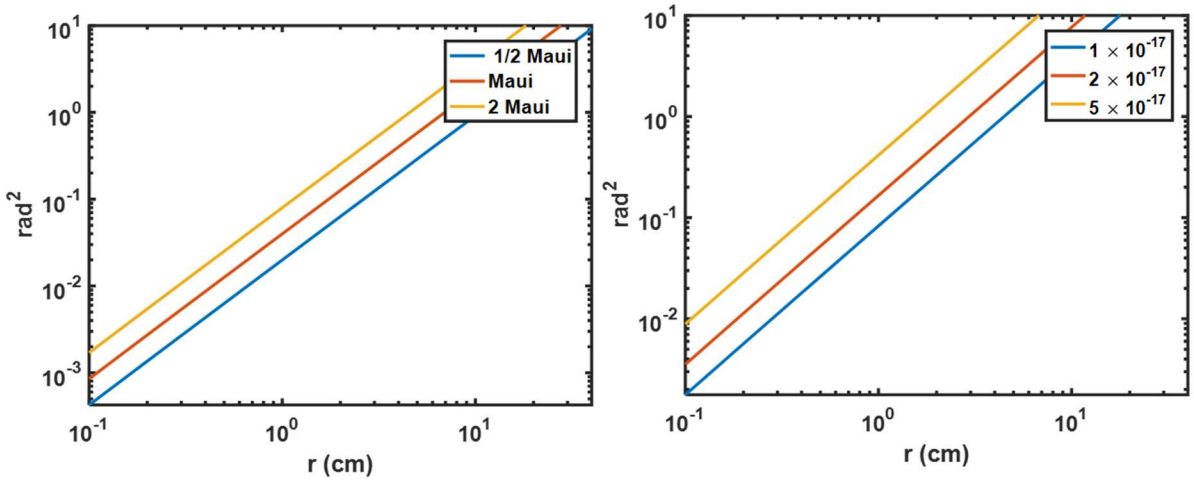

Fig. 7. HWSF evaluated for the isoplanatic (left) and anisoplanatic (right) conditions described in Table 1 and 2. In this figure spatial separation is varied while the angular separation is fixed as $\vartheta = 0$

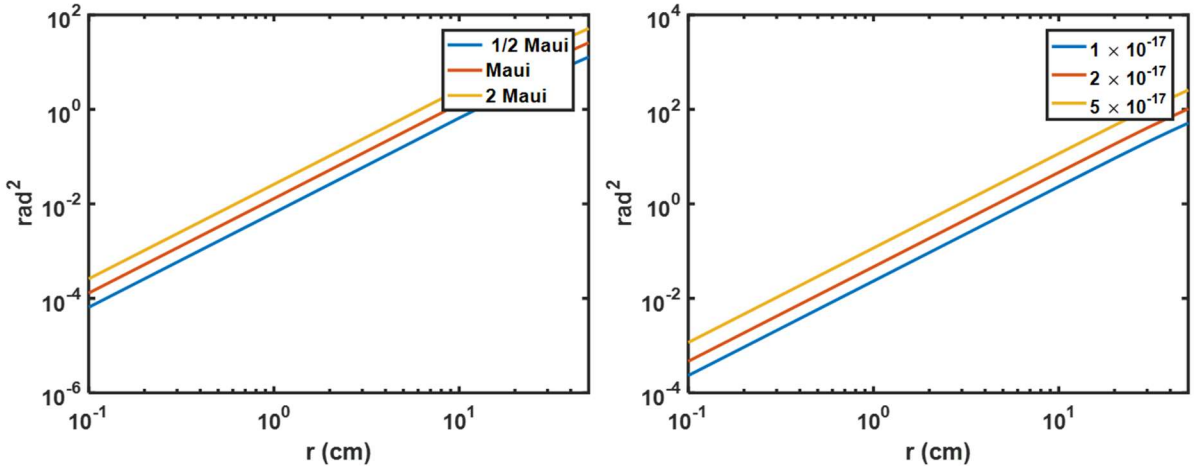

Fig. 8. HWSF evaluated for the isoplanatic (left) and anisoplanatic (right) conditions described in Table 1 and 2. In this figure spatial separation is varied while the angular separation is fixed as $\vartheta = 10$ μrad

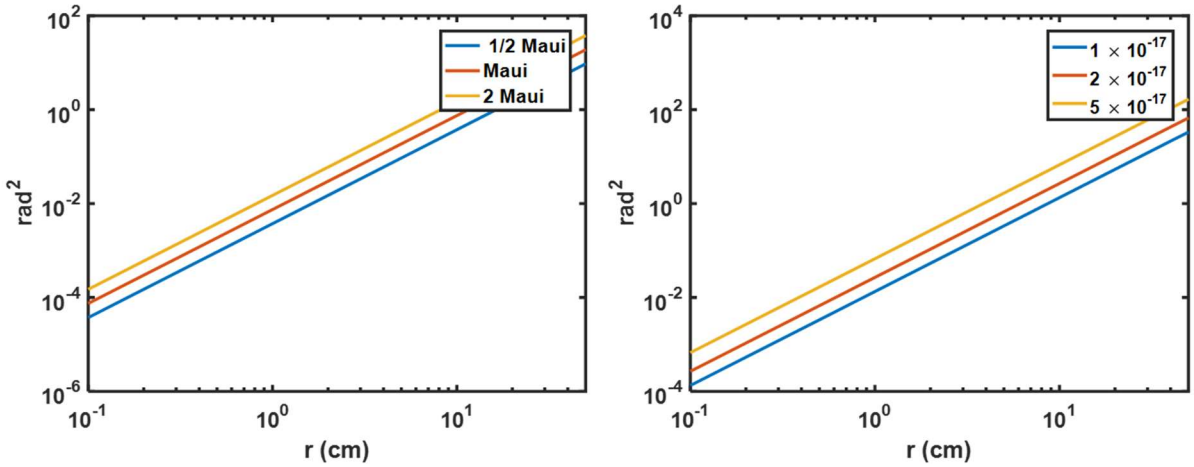

Fig. 9. HWSF evaluated for the isoplanatic (left) and anisoplanatic (right) conditions described in Table 1 and 2. In this figure spatial separation is varied while the angular separation is fixed as $\vartheta = 50$ μrad

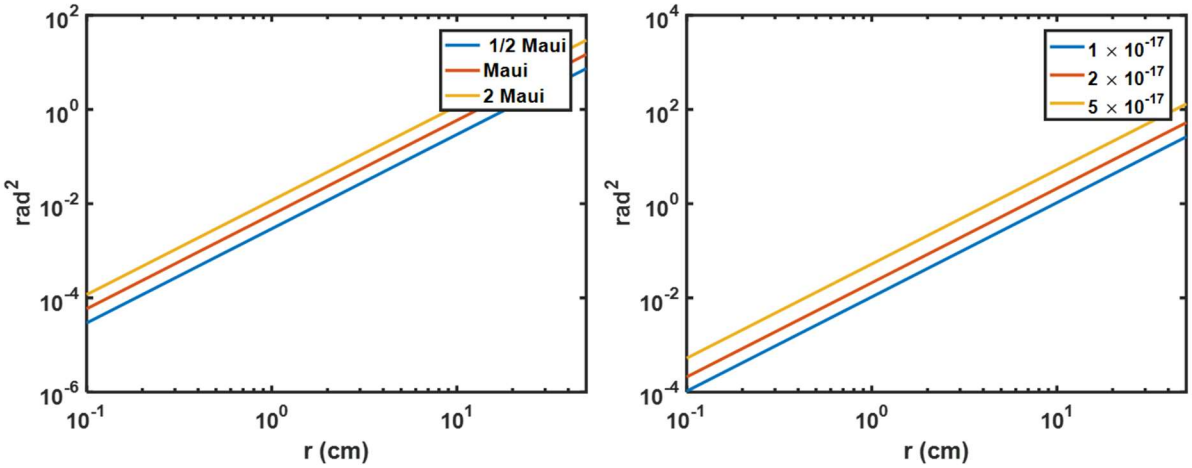

Fig. 10. HWSF evaluated for the isoplanatic (left) and anisoplanatic (right) conditions described in Table 1 and 2. In this figure spatial separation is varied while the angular separation is fixed as $\vartheta = 100$ μrad

4. CONCLUSIONS

In this paper, I have taken a first step in understanding the effect of atmospheric turbulence on the light-field and LF imaging. The primary contribution of this work is the re-introduction of the HWSF as described by Fried in that context. Also, I have performed a preliminary evaluation of the HWFS for two scenarios with similar integrated turbulence strengths but differing values of the isoplanatic angle; values for one scenario were several times larger. I found that when the separation angle is held constant and spatial separation increased the HWSF (in terms of mean-squared phase difference) increases approximately according to a square-law. On the other hand, when separation is held constant and the HWSF evaluated as angular separation increases the mean-squared decreases following a power law around 0.8. Apart from a bulk increase in the mean-squared difference in phase there is no observed change is behavior of the HWSF between anisoplanatic (horizontal) and isoplanatic (mountaintop) view conditions. The likely takeaway being that extreme anisoplanatism is an effect of the imaging system relative to the imaging conditions rather than the turbulence volume.

5. REFERENCES

1. Archer, G.E., J.P. Bos, and M.C. Roggemann, *Comparison of bispectrum, multiframe blind deconvolution and hybrid bispectrum-multiframe blind deconvolution image reconstruction techniques for anisoplanatic, long horizontal-path imaging.* Optical Engineering, 2014. **53**(4): p. 043109-043109.
2. Bos, J.P. and M.C. Roggemann, *Robustness of speckle-imaging techniques applied to horizontal imaging scenarios.* Optical Engineering, 2012. **51**(8): p. 083201-1-083201-18.
3. Roggemann, M.C. *Wave Front Correction and Post-Detection Image Reconstruction Under Anisoplanatic Conditions with a Scene-Based Wave Front Sensor*. in *Propagation Through and Characterization of Atmospheric and Oceanic Phenomena*. 2016. Optical Society of America.
4. Jefferies, S.M., et al. *High-resolution imaging through strong atmospheric turbulence*. in *Proc. SPIE*. 2013.
5. Gabriel, L., *La photographie intégrale.* Comptes-Rendus, Académie des Sciences, 1908. **146**: p. 446-551.
6. Adelson, E.H. and J.Y. Wang, *Single lens stereo with a plenoptic camera.* IEEE transactions on pattern analysis and machine intelligence, 1992. **14**(2): p. 99-106.
7. Ng, R., et al., *Light field photography with a hand-held plenoptic camera.* Computer Science Technical Report CSTR, 2005. **2**(11): p. 1-11.
8. Srinivasan, P.P., R. Ng, and R. Ramamoorthi, *Light Field Blind Motion Deblurring.* arXiv preprint arXiv:1704.05416, 2017.
9. Ragazzoni, R., *Pupil plane wavefront sensing with an oscillating prism.* Journal of modern optics, 1996. **43**(2): p. 289-293.
10. Rodríguez, J., et al. *The CAFADIS camera: a new tomographic wavefront sensor for Adaptive Optics*. in *1st AO4ELT conference-Adaptive Optics for Extremely Large Telescopes*. 2010. EDP Sciences.

11. Rodríguez-Ramos, L.F., et al. *The Plenoptic Camera as a wavefront sensor for the European Solar Telescope (EST)*. in *Proc. SPIE*. 2009.
12. Wu, C., J. Ko, and C.C. Davis, *Determining the phase and amplitude distortion of a wavefront using a plenoptic sensor.* JOSA A, 2015. **32**(5): p. 964-978.
13. Fried, D.L. *Angular dependence of atmospheric turbulence effect in speckle interferometry*. in *International Astronomical Union Colloquium*. 1979. Cambridge University Press.
14. Fried, D.L., *Spectral and angular covariance of scintillation for propagation in a randomly inhomogeneous medium.* Applied optics, 1971. **10**(4): p. 721-731.
15. Tatarskii, V.I., *Wave propagation in turbulent medium.* Wave Propagation in Turbulent Medium, by Valerian Ilich Tatarskii. Translated by RA Silverman. 285pp. Published by McGraw-Hill, 1961., 1961.
16. Fried, D.L., *Limiting resolution looking down through the atmosphere.* JOSA, 1966. **56**(10): p. 1380-1384.
17. Fried, D.L., *Anisoplanatism in adaptive optics.* JOSA, 1982. **72**(1): p. 52-61.